

High-throughput metal nanoparticle catalysis by pulsed laser ablation

Selim Senkan^{a,*}, Michael Kahn^a, Shici Duan^a, Anna Ly^b, Craig Leidholm^b

^aDepartment of Chemical Engineering, University of California, Los Angeles, CA 90095, USA

^bLaboratory Catalysts Systems, Los Angeles, CA 90024, USA

Available online 18 July 2006

Abstract

A high-throughput pulsed laser ablation (HT-PLA) system was developed to rapidly prepare uniformly sized single- and multi-metallic nanoparticles with different diameters for catalytic applications. Catalytic materials containing Rh, bimetallic Rh/Pt and trimetallic Rh/Pt/Au nanoparticles were synthesized from targets prepared by blending, tableting and sintering powders of pure metals, and by directly collecting the nanoparticles created on support materials. Nanoparticles exhibited crystallinity and uniformity in size and composition as determined by high-resolution transmission electron microscopy (HR-TEM) and energy dispersive X-ray (EDX) spectroscopy, respectively. The supported nanoparticles created by HT-PLA were also screened for their catalytic activities and selectivities for the partial oxidation of propylene. In less than a day, over 40 different catalytic materials of nanoparticles supported on γ -Al₂O₃, CeO₂, TiO₂, SiO₂ and Y-ZrO₂ were prepared and evaluated. This highly streamlined approach resulted in the discovery of TiO₂ supported 0.004% Rh nanoparticles as a promising new lead for the synthesis of partial oxidation products of propylene with one-pass yields of about 13% at 275 °C.

© 2006 Published by Elsevier B.V.

Keywords: Combinatorial chemistry; Heterogeneous catalysis; Metal nanoclusters

1. Introduction

Heterogeneous catalysts are used in the manufacture of a vast array of chemicals and fuels, and as such significantly contribute to our economy and high living standards [1,2]. However, in spite of their importance and broad utility, the development of new and improved catalysts continues to be an arduous and challenging task [1,3]. Supported metal particles (clusters of atoms) are among the most important catalysts used in industry today, and it is well established that their catalytic behavior, i.e. reactivity and selectivity, is influenced by the particle size, composition and by their interactions with the support [4–6]. For example, 2–3 nm particles of Au supported on TiO₂ were shown to be highly selective towards the formation of propylene oxide from propylene, hydrogen and oxygen [5]. On the other hand, larger Au nanoparticles result in the total oxidation of propylene to CO₂, while smaller clusters produce propane [5]. Consequently, a large number of techniques have been proposed or developed to create uniformly sized nanoparticles of metals and metal oxides dispersed over substrates. Examples include the sol–gel method, liquid precipitation and colloidal micelles [7], as well as

vaporization/condensation, aerosol and flame synthesis [8], and electron beam lithography and photolithography [9]. However, in spite of substantial efforts expended to develop these techniques, their impact on industrial heterogeneous catalysis has been insignificant due to complex preparation steps involved and/or slow rates of production. In addition, most of the techniques have also proved to be difficult for the preparation of *multi-metallic* nanoparticles that are *anchored* to the support materials.

Pulsed laser ablation (PLA) ameliorates most of these problems, and represents a highly versatile and powerful approach for the preparation of *uniformly sized multi-metallic nanoparticles* for catalytic applications. Laser ablation is a phenomenon in which material is ejected from a solid surface as a consequence of rapid energy deposition by light irradiation [10]. Rapid energy deposition results in surface heating and ionization leading to coulombic and thermal explosion concomitant with the formation of high temperature (i.e. plasma) gas and shock waves. PLA is already being exploited in a number of technological applications such as small device fabrication, pulsed laser deposition (PLD) of thin films and coatings [11], laser surgery [12] and matrix assisted laser desorption ionization (MALDI) [13].

PLA is suitable for the synthesis of catalytic metallic nanoparticles for a number of reasons. First, virtually any metal or mixtures in any composition and form, e.g. sheet, film,

* Corresponding author. Fax: +1 310 267 0177.

E-mail address: Senkan@ucla.edu (S. Senkan).

powder, can be transformed into nanoparticles with a reasonably narrow size distribution using high power pulsed lasers [10]. Consequently, PLA avoids the use of dangerous or expensive liquid or gaseous precursor chemicals. Second, nanoparticles prepared by PLA can directly be collected on catalyst supports, thereby eliminating the need to handle potentially toxic nanopowders. Since nanoparticles can be created with a significant number of dangling bonds, because they originate from a high temperature plasma gas, they can be strongly adsorbed, thus become anchored on supports. This decreases their mobility and inhibits particle sintering during reactions. This is a distinct advantage of PLA compared to solution based methods that tend to passivate particle surfaces by moieties present in the reaction medium. Third, PLA creates no byproducts and can be scaled up for industrial applications. Finally, the sizes and the compositions of the nanoparticles generated by PLA can be adjusted to generate materials for specific catalytic and other applications.

Although metal alloys are the preferred form of targets for the synthesis of multi-metallic nanoparticles using PLA, the limited availability of alloys restricts the compositions of nanoparticles that can be readily created. Here we report a versatile and high-throughput technique to prepare multi-metallic nanoparticles from commercially available powders of pure metals. The method developed involves the preparation of multi-metallic target tablets first by blending, cold pressing and *sintering* fine powders (preferably nanometer sized powders) of individual metals, followed by the synthesis of multi-metallic nanoparticles by high-throughput PLA (HT-PLA) of the target. Sintering promotes interparticle diffusion of metals and results in alloy formation, and also creates stronger target tablets that perform better under PLA conditions. Sintering can be accomplished under an inert gas, such as He, Ar, or a reactive gas such as H₂ to remove oxide layers. In addition, sintering and alloy formation can also be accomplished by laser heating the target surface prior to ablation. The creation of multi-metallic nanoparticles having the same composition as the target tablet requires: (1) stoichiometric ablation of the target which is accomplished by rapidly heating the surface of the target and (2) rapid supercooling of the hot plasma gas mixture. The former requires the use of high power and short pulse-length lasers having focal beam diameters that are significantly larger than the diameters of the individual metal particles used to prepare the target tablet. Short pulse length decreases thermal diffusion into the solid target and improves stoichiometric ablation. Small target metal particle diameters are preferred for the generation of multi-component nanoparticles. Rapid supercooling results in the nucleation and growth of multi-metallic nanoparticles having the same composition as the multi-component hot plasma gas. The latter is accomplished by operating the HT-PLA under a low pressure inert gas atmosphere. Reactive ambient gas such as O₂ can also be used for the production of metal oxide nanoparticles. Only when the above requirements are met that nanoparticles possess similar composition as the target. However, target compositions can systematically be varied to achieve the desired nanoparticle compositions when the above conditions are not present.

2. Experimental

In Fig. 1, the HT-PLA system developed is shown. The setup consists of a rotatable target holder that houses multiple targets (24 cylindrical targets with 1.25 cm diameters in the current design). The target under laser illumination is continuously spun at a rate of about 5–10 rpm for the better utilization of the target material. A pulsed laser beam (Lambda Physik Compex 100 Excimer Laser, 300 mJ/pulse, 30 ns pulse duration) is focused to a spot of about 0.1 cm diameter, off axis on the surface of the target, arriving at an angle of about 45°. Nanoparticles created in the ablation plume are then collected either on support pellets (0.4 cm diameter × 0.1 cm thick cylinders), on standard transmission electron microscope (TEM) grids, or single crystal silicon wafers as shown in Fig. 1. Consequently, it is possible to readily characterize the nanoparticles before reaction screening. In the current design, a rotatable holder is used to house up to 30 support pellets and/or TEM grids. A mask prevents cross contamination of the sites. The distance between the target and collection site can also be adjusted. This assembly is placed inside a gas tight (vacuum) chamber to control the ambient gas conditions during PLA (Ar in the present experiments). The laser beam is introduced into the chamber through a UV transparent fused silica window. The size and composition of the nanoparticles formed in PLA are primarily determined by the laser power density (i.e. fluence, energy of the photons and pulse duration), the nature and

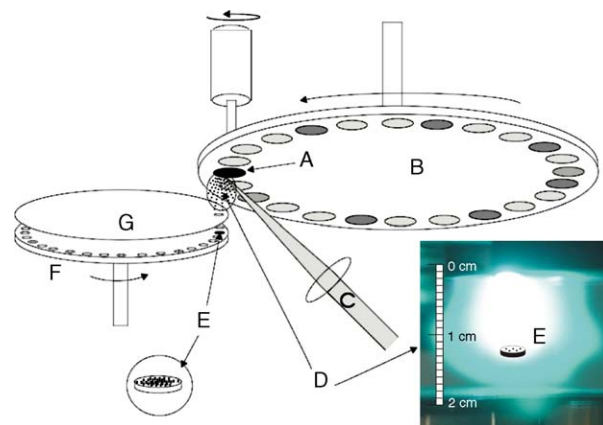


Fig. 1. A sketch of the high-throughput pulsed laser ablation (HT-PLA) system that enables the rapid preparation of a large number of supported multi-metallic nanoclusters: (A) ablating target, (B) rotatable (selectable) target holder, (C) pulsed laser beam, (D) ablation plume, (E) catalyst support or TEM grid containing nanoparticles, (F) catalyst support or TEM grid holder and (G) mask. All the components are placed in a gas tight (vacuum) chamber for the control of pressure and the nature of the ambient gas. A multitude of different targets (24 shown) can be ablated sequentially, and the nanoparticles created can be deposited directly on support pellets or TEM grids. The pellets can then be used for catalytic screening. A mask is used to prevent cross contamination of sites. The distance between the target and support pellets can also be adjusted. The pulsed laser beam enters the chamber through a fused silica window and irradiates the target at a 45° angle. The target under illumination is continuously spun at 5–10 rpm for the better utilization of the target material. Also shown is a rhodium metal ablation plume showing the target and schematic collection of nanoparticles on the external surface of support pellets, TEM grids or silicon wafers, by placing them inside the plume.

density of the ambient gas in the ablation chamber [10], and the distance from the target surface. Other parameters, such as the light absorbance, heat capacity, enthalpy of vaporization, boiling point and thermal conductivity of the target also influence the properties of the nanoparticles. The HT-PLA system reported here enables the systematic exploration of all of these variables within a single experiment, and allows the rapid determination of conditions under which the synthesis of nanoparticles suitable for specific catalytic applications can be accomplished.

An actual picture of a Rh ablation plume is also shown in Fig. 1. It is particularly important to note that in PLA nanoparticles are deposited on the external surfaces of the support materials, without penetration into their pores. Consequently, catalyst screening is accomplished in the absence of pore-diffusion limitations. In other words, catalytic materials prepared by PLA can be evaluated under identical intrinsic reaction rate limited, i.e. transport free conditions, thus their rank order can be obtained unambiguously. This is another advantage of PLA compared to other catalyst preparation methods.

3. Results and discussion

In Fig. 2, TEM pictures of Rh nanoparticles collected on carbon film are shown as function of distance along the ablation plume, together with their corresponding number statistics and number densities (see Fig. 1, inset for a spatial reference). Fig. 3 clearly shows a narrow and adjustable particle size distribution, with particle diameters decreasing with distance from the target. Mean particle diameters were about 6, 3 and 1 nm, at 1.3, 1.6 and 1.9 cm from the target, respectively. It is interesting to note that the particle size distributions also become narrower with increasing distance from the target.

In Fig. 3, the high-resolution TEM (HR-TEM) images of bimetallic Rh/Pt and trimetallic Rh/Pt/Au nanoparticles created by the HT-PLA system are shown, together with representative EDX spectra. These particles were created from tablets prepared by blending and pressing 325 mesh 99.9% pure metal powders at approximate weight ratios of 50/50 and 40/40/20 for the Rh/Pt and Rh/Pt/Au cases, respectively, followed by sintering at 700 °C for 20 min under Ar gas. The images in Fig. 3 correspond to nanoparticles collected at about 2 cm from

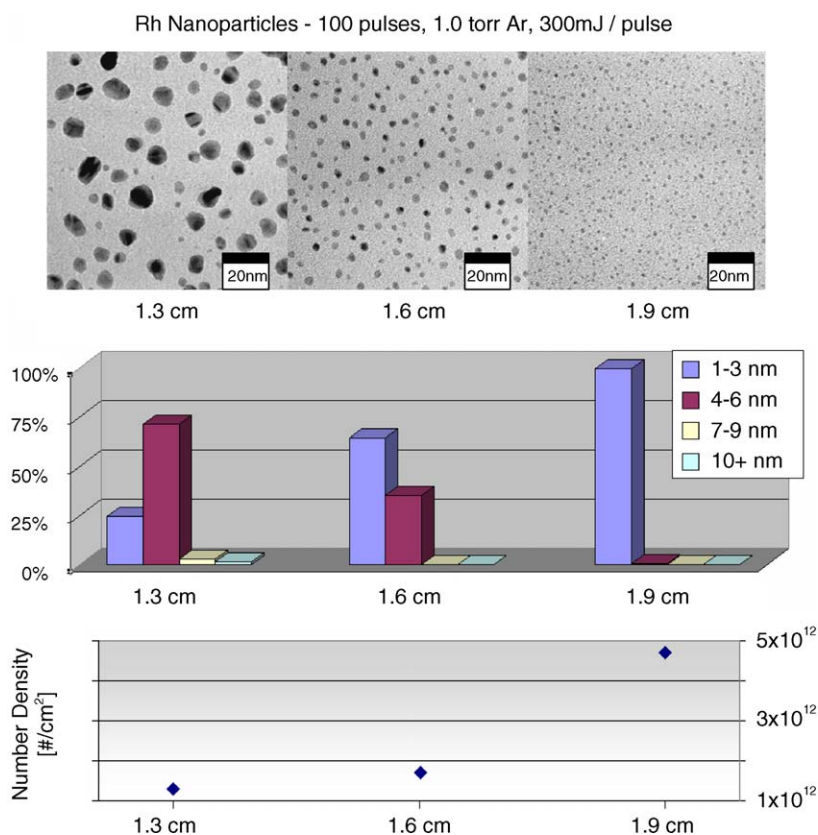


Fig. 2. Rhodium metal nanoparticles collected on carbon film at 1.3, 1.6 and 1.9 cm along the ablation plume (see Fig. 1 for spatial reference). Ablation conditions were the following: 100 pulses, 248 nm KrF excimer laser operating at 300 mJ/pulse and 30 ns pulse width, 1 Torr Ar ambient pressure. On top are the TEM images (JEOL JEM-2000FX), which clearly show that particle diameters decrease with increasing distance from the target. The black line inserts correspond to 20 nm scale. Particle number statistics shown in the middle figure clearly support this trend. For example, the fractions of smaller particles (1–3 nm) increase, while those for 4–6 nm and larger decrease with distance along the ablation plume. In contrast, the number densities of particles steadily increase along the plume, consistent with the fragmentation of energetic larger particles into smaller ones and/or nucleation and growth of new particles. Acquisition of TEM images below 1.3 cm was not possible because of carbon film destruction by the larger energetic particles. However, stronger single crystal silicon wafers were used to collect particles early in the plume, followed by atomic force microscopy (AFM) to characterize them. The AFM analysis of a sample acquired at 1.0 cm indicated the presence of particles larger than those observed at 1.3 cm.

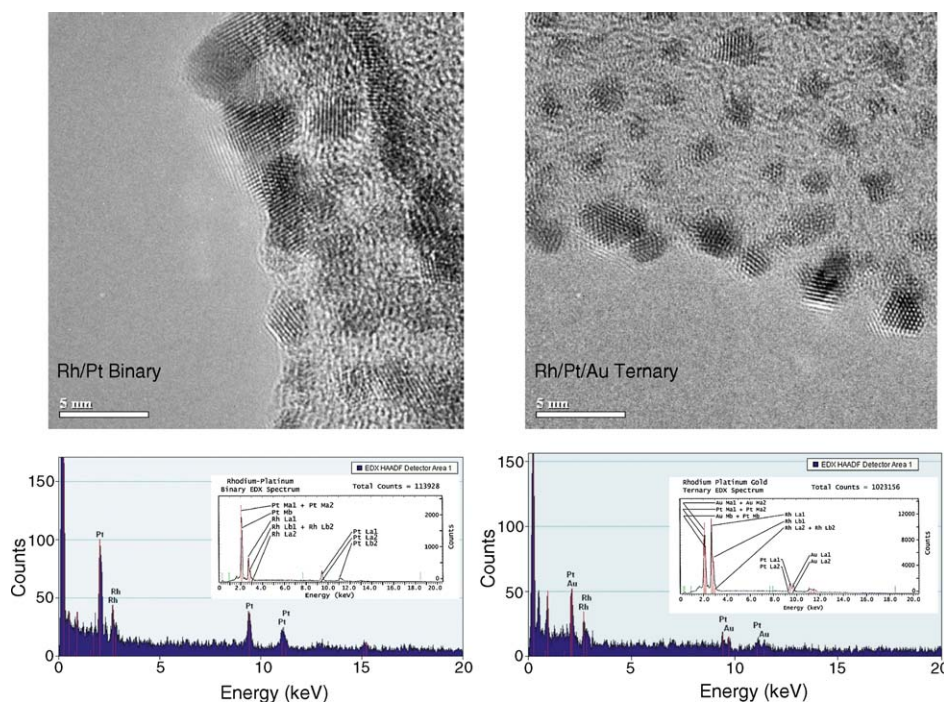


Fig. 3. High-resolution transmission electron microscope (HR-TEM) images of bimetallic Rh/Pt (left) and trimetallic Rh/Pt/Au (right) nanoparticles created by HT-PLA and determined by high-resolution TEM (FEI Tecnai TF30UT, 300 kV HT, FEG source with ultra twin lens) and the corresponding representative energy dispersive X-ray (EDX) spectra of *individual particles*, where Cu peaks corresponding to the TEM grid were removed for clarity. The EDX spectra of the targets, determined separately using a SEM (Cambridge Stereoscan 250) are also presented as inserts. The similarity of EDX spectra suggests that the compositions of the nanoparticles formed are similar to those of the corresponding target materials. As evident from these pictures, nanoparticles were crystalline, with particle diameters in the 1–3 nm range. The EDX spectra also indicate the presence of all the constituent metals within the nanoparticles. The EDX analysis of several distinct particles also exhibited similar spectra, indicating the compositional similarity of different nanoparticles.

the target for 100 pulses, while keeping all other variables constant. As evident from this figure, the particles were crystalline and uniformly sized with diameters in the range of 1–3 nm. This size range is suitable for catalysis [4–6], and was also determined to be nearly independent of the number of laser pulses used, as long as the fractional surface coverage remains small. At high surface coverages, the probability for nanoparticles to land on top of each other increases, thereby increasing the particle diameter. However, even when a second particle lands on and sinters with a surface particle of the same volume, resulting particle diameter increase would only be 25% (i.e. to $2^{1/3}$). An examination of the EDX analysis shown in Fig. 3 confirms that the nanoparticles possess all the constituent metals used in their preparation. In addition, the EDX analysis of several distinct nanoparticles for each of the bimetallic and trimetallic cases also exhibited similar spectra to those shown in Fig. 3, suggesting that all the nanoparticles should have a similar overall composition. We also performed EDX analysis of the target materials using a scanning electron microscope (SEM), and these results are presented as inserts in the nanoparticle EDX spectra in Fig. 3. As evident from these results, the EDX spectra of the individual nanoparticles were qualitatively similar to those of the corresponding target materials, both for the binary and ternary cases. This similarity suggests that the individual nanoparticles possess compositions that are close to the corresponding targets. Metal weight ratios were also extracted from each EDX spectra, using software and

built-in standards, to better compare the compositions of the nanoparticles and the targets. The metal weight ratios for the targets and for the nanoparticles were approximately 33/67 and 24/76 for the Rh/Pt binary, and 28/53/18 and 21/66/13 for the Rh/Pt/Au ternary systems, respectively. These findings are reasonable considering the fact that the spatial variation of the target composition, shot-to-shot laser power fluctuations, together with varying EDX cross sections and matrix effects render quantitative analysis of single nanoparticles by EDX difficult. Nevertheless, the results clearly support the fact that nanoparticles created by HT-PLA possessed all the metals present in the original target at a similar composition.

Next, the HT-PLA was integrated with array channel microreactors and mass spectrometry (MS) [14] for the catalytic evaluation of supported metal nanoparticles for the industrially important reaction of propylene partial oxidation. For this, we prepared over 40 different catalytic materials consisting of nanoparticles of Rh, binary Rh/Pt and ternary Rh/Pt/Au supported on porous pellets of γ - Al_2O_3 (BET surface area 128 m^2/g), CeO_2 (17 m^2/g), TiO_2 (268 m^2/g), SiO_2 (325 m^2/g) and Y-Zr O_2 (37 m^2/g) at about 2 cm in the ablation plume. Different metal loadings were achieved by using 1, 10, 100 and 1000 laser pulses. The preparation of these 40 catalytic materials took approximately 3 h.

Catalyst evaluation was performed under atmospheric pressure and at temperatures of 250, 275 and 300 °C using a feed stream of 20% propylene (PR) and $\text{C}_3\text{H}_6/\text{O}_2$ ratios of 0.25,

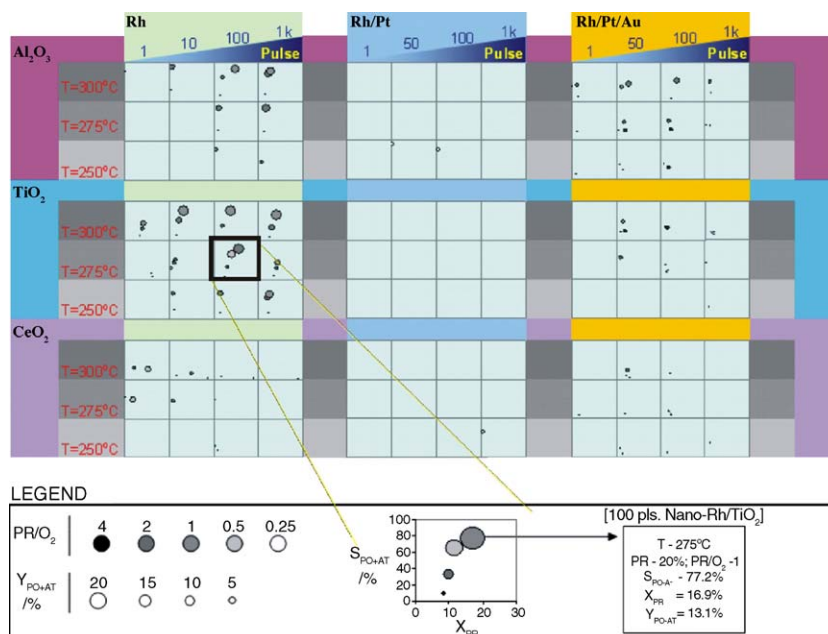


Fig. 4. Selected results for mass 58 production, i.e. propylene oxide (PO) + acetone (AT), on γ - Al_2O_3 , TiO_2 and CeO_2 supported nanoparticles of Rh, binary Rh/Pt and ternary Rh/Pt/Au displayed in a multi-dimensional matrix format. In each square, mass 58 selectivity ($S_{\text{PO+AT}}$) vs. propylene (PR) conversion (X_{PR}) is plotted for one catalyst, with PO + AT yields ($Y_{\text{PO+AT}} = S_{\text{PO+AT}} \cdot X_{\text{PR}}$) presented by the sizes of the circles or spots (see legend). Different circles in each square correspond to different $\text{C}_2\text{H}_6/\text{O}_2$ ratios used in the experiments, in accordance with the gray scale shown in the legend. Within each group, columns from left to right correspond to increased nanoparticle loadings, corresponding to increased number of laser pulses (1, 10, 100 and 1000 pulses). Different rows correspond to different reaction temperatures (250, 275 and 300 °C) for each support material as indicated. The pressure was atmospheric with GHSV of 20,000 h^{-1} . Among all the catalytic materials considered, TiO_2 supported 100 pulse Rh was the best performer producing PO + AT at a yield of 13% at 275 °C, details of which are shown in the legend section. Multi-metallic materials exhibited poor PO + AT yields because of excessive combustion by Pt. The presence of optimal nanoparticle loading is evident for single Rh loading on TiO_2 at 300 °C. The decrease in selectivity and yield at high laser pulses is likely due to increased particle overlap thus film formation.

0.5, 1, 2 and 4, with the balance being helium. The gas hourly space velocity (GHSV) was 20,000 h^{-1} . The partial oxidation of propylene can form a variety of products such as propylene oxide (PO), acetone (AT), acrolein (AC) and propanal (PaL) [15]. Consequently, a matrix inversion technique was used to deconvolute the mass spectrometric (MS) signals and to arrive at measurements that were directly attributable to different products [15]. However, because the deconvolution of the mass spectral signals for PO and AT is not unique, they were reported together as mass 58 signals. The screening experiments were completed in about 3 h.

In Fig. 4, selected results from these screening experiments are presented in a multi-dimensional matrix format. As defined in the figure caption, larger spots correspond to higher PO + AC yields (mass 58), thus are desirable. As can be seen in Fig. 4, supported single Rh nanoparticles were the best performers among all the different catalytic materials evaluated, and these results are presented in the first column. In particular, TiO_2 supported Rh nanoparticles at 100 pulse loading led to the highest yield ($Y_{\text{PO+AT}}$) of 13% at 275 °C in our experiments, which is also indicated in the legend. This yield surpasses the performance of any binary or ternary metal combinations considered. The 100 pulses of Rh nanoparticles deposited on TiO_2 correspond to about 0.004 wt% Rh, based on TEM measurements, and by assuming 3 nm diameter spherical particles of Rh in cubic packing. The 13% yield is a superior result when compared to the performance of 1% Rh/ TiO_2

catalysts prepared by impregnation which only produced about 1% PO + AT yield under identical reaction conditions [15]. Nanoparticle catalysis results reported here therefore represent a significant improvement over impregnation with regard to the utilization of the expensive Rh metal. The fact that nanoparticles remained on the outer surfaces of the pellets, i.e. egg shell structure, was also advantageous from an engineering point of view because such catalysts will be less prone to pore-diffusion limitations, especially for the case of highly exothermic reactions such as partial oxidations. The observation of 13% PO + AT yield at only 0.004% Rh loading, i.e. at very low nanoparticle loadings, is particularly encouraging with respect to the scale up of the HT-PLA for industrial catalysis applications. Representative results for the supported multi-metallic nanoparticles are also presented in Fig. 4. The poor performances of these multi-metallic catalysts were due to excessive CO_2 formation, induced by the presence of Pt, which is a well-known combustion catalyst [2,3].

The results presented in Fig. 4 also illustrate several catalytic insights. Most importantly, the PO + AT selectivities and yields of TiO_2 supported Rh exhibited an optimal loading of 100 pulses, which was most apparent at 300 °C. This optimal performance can readily be explained by the presence of low number of nanoparticles or catalytic sites at lower Rh loadings, and by particle agglomeration and possibly film formation, thus loss of nanoparticle features, at higher number of laser pulses. This explanation is in harmony with the TEM images presented

in Fig. 3, although the porosity of the support materials complicates this picture. Such a trend was also observed with other supports and metals, albeit at lower PO + AT yields. Selectivities for PO + AT also were noted to exhibit maxima with regard to the C_3H_6/O_2 ratio, with the highest PO + AT selectivities observed at 1. At higher C_3H_6/O_2 ratios, O_2 limits C_3H_6 conversion, while at low C_3H_6/O_2 ratios excessive deep oxidation sets in as evidenced by CO_2 formation.

In summary, the HT-PLA has been shown to be a versatile technique for the rapid creation of multi-metallic nanoparticles that are crystalline and uniform in size and composition, from readily available powders of pure metals. Since the amount of metals used in the creation of nanoparticle catalysts is small, HT-PLA can readily be scaled up to have an impact on industrial heterogeneous catalysis. The HT-PLA, in conjunction with high-throughput catalyst screening methods, has also been shown to significantly increase the tempo of research for the discovery and optimization of supported nanoparticle catalysts, as demonstrated by the discovery of new leads for the propylene partial oxidation reactions.

Acknowledgements

This research was funded, in part, by the US Environmental Protection Agency and the National Science Foundation. The authors also would like to thank Allen Lu and Patrick Rivers for their help with the PLA chamber construction and sintering work, respectively.

References

- [1] National Institute of Standards and Technology, Advanced Technology Program, Catalysis and Biocatalysis, White Paper, 1998
M.E. Davis, Future directions in catalysis: structures that function at the nanoscale, in: NSF Workshop, June 19–20, 2003;
J.M. White, Opportunities for catalysis in the 21st century, in: Basic Energy Sciences Advisory Committee Subpanel Workshop, Department of Energy, May 14–16, 2002.
- [2] National Research Council, Catalysis Looks to the Future, National Academy Press, Washington, DC, 1992.
- [3] G. Poncelet, J. Martens, B. Delmon, P.A. Jacobs, P. Grange (Eds.), Preparation of Catalysts VI, Elsevier, Amsterdam, The Netherlands, 1995
- [4] O.S. Alexeev, B.C. Gates, *Ind. Eng. Chem. Res.* 42 (2003) 1571.
- [5] T. Hayashi, K. Tanaka, M. Haruta, *J. Catal.* 178 (1998) 566.
- [6] M. Valden, X. Lai, D.W. Goodman, *Science* 281 (1998) 1647.
- [7] J.D. Aiken, R.G. Finke, *J. Mol. Catal. A. Chem.* 145 (1999) 1.
- [8] M.T. Swinehart, *Curr. Opin. Colloid Interface Sci.* 8 (2003) 127.
- [9] A. Avoyan, G. Rupprechter, A.S. Eppler, G.A. Somorjai, *Top. Catal.* 10 (2000) 107.
- [10] W. Marine, L. Patrone, B. Luk'yanchuk, M. Sentis, *Appl. Surf. Sci.* 154–155 (2000) 345;
L.V. Zhigilei, *Appl. Phys.* A76 (2003) 339.
- [11] M.N.R. Ashfold, F. Claeysens, G.M. Fuge, S.J. Henley, *Chem. Soc. Rev.* 33 (2004) 23.
- [12] E.L. Tanzi, J.R. Lupton, T.S. Alster, *J. Am. Acad. Dermatol.* 49 (2003) 1;
S.C. Gibson, D.S. Bryne, A.J. McKay, *Br. J. Surg.* 91 (2004) 893.
- [13] G. Corana, G. Toffoli, *Comb. Chem. High Throughput Screen* 7 (2004) 707.
- [14] S. Senkan, *Angew. Chem. Int. Ed.* 40 (2001) 312;
S.M. Senkan, S. Ozturk, *Angew. Chem. Int. Ed.* 38 (1999) 791;
S.M. Senkan, K. Krantz, S. Ozturk, V. Zengin, I. Onal, *Angew. Chem. Int. Ed.* 38 (1999) 2794.
- [15] T. Miyazaki, S. Ozturk, I. Onal, S. Senkan, *Catal. Today* 81 (2003) 473.